ELSEVIER

www.elsevier.nl/locate/jorganchem

Journal of Organometallic Chemistry 596 (2000) 77–83

Journal of Organometallic Chemistry

The metal–metal bond in the dibenzotetramethyltetraaza[14]annulene–ruthenium dinuclear complex: a structural, magnetic, and theoretical analysis

Joëlle Hesschenbrouck [a], Euro Solari [a], Rosario Scopelliti [a], Carlo Floriani [a,*], Nazzareno Re [b]

[a] *Institut de Chimie Minérale et Analytique, BCH, Université de Lausanne, CH-1015 Lausanne, Switzerland*
[b] *Facoltà di Farmacia, Università degli Studi 'G. D'Annunzio', I-66100 Chieti, Italy*

Received 23 June 1999

Dedicated to Professor F. Albert Cotton in the occasion of his 70th birthday. We thank him for being the academic mentor of our science

Abstract

The thermal decomposition of [{Ru(tmtaa)}$_2$(1,5-cyclooctadiene)] (**1**) in boiling toluene has led to the formation of the metal–metal bonded dinuclear complex [{Ru(tmtaa)}$_2$] (**2**), (Ru–Ru, 2.3829(4) Å). Upon oxidation using Cp_2FeBPh_4, the corresponding monocation [{Ru(tmtaa)}$_2$]BPh_4 (**3**) is synthesized with an Ru–Ru bond distance of 2.2782(4) Å. The magnetic measurements of **2** and **3** are in agreement with a ground state $s=1$ and $s=\frac{1}{2}$, respectively. Calculations indicate an Ru–Ru $\sigma^2\pi^4\delta^2\delta^{*2}\pi^{*2}$ electron configuration and suggest an Ru–Ru double bond character for **2**, while the significant shortening by 0.105 Å of the Ru–Ru distance in **3** is in agreement with a $\sigma^2\pi^4\delta^2\delta^{*2}\pi^{*1}$ electron configuration and an Ru–Ru bond order of 2.5. Complex **2** serves as a source of the [Ru(tmtaa)] fragment in a variety of reactions, one of which is the reaction with ethylene in THF leading to the quite rare ethylene diamagnetic complex [Ru(tmtaa)(THF)(η^2-C_2H_4)] (**4**), (Ru···(η^2-C_2H_4), 2.009(2); C–C, 1.384(5) Å). © 2000 Elsevier Science S.A. All rights reserved.

Keywords: Ru–Ru bonds; Ru–macrocycle; Ru–ethylene; Tetramethyltetraaza[14]annulene

1. Introduction

The chemistry of the [Ru=Ru] functionality has been intensely investigated in the context of Ru–porphyrin derivatization [1–3]. However, such functionalities have not received the appropriate attention when ruthenium was bonded to other macrocycles or polydentate ligands. More than 20 years ago, Goedken et al. published a very short communication on the metal–metal bonded dinuclear complex $[Ru_2(tmtaa)_2]^{0/+}$ (tmtaa = dibenzotetramethyltetraaza[14]annulene dianion) [4,5], without providing details of the structure and the magnetic behavior [6]. Such a metal–metal bonded dinuclear complex can be considered as the appropriate source of the [Ru(tmtaa)] monomer, which has been recently found to display a quite rich Ru–carbene chemistry [7]. A high-yield synthetic methodology for $[Ru_2(tmtaa)_2]$ has been developed for the synthesis of quantities suitable for reactivity studies. Its oxidation to the corresponding cationic species $[Ru_2(tmtaa)_2]^+BPh_4^-$ has been performed as well as its transformation into the monomeric Ru–ethylene complex. A detailed structural, magnetic, and theoretical analysis is reported for the three complexes.

2. Results and discussion

2.1. Synthesis, structure, and magnetism

The synthesis of the metal–metal bonded dinuclear complex **2** has been performed via a thermal displace-

* Corresponding author. Tel.: +41-21-6923902; fax: +41-21-6923905.
E-mail address: carlo.floriani@icma.unil.ch (C. Floriani)

0022-328X/00/$ - see front matter © 2000 Elsevier Science S.A. All rights reserved.
PII: S0022-328X(99)00542-2

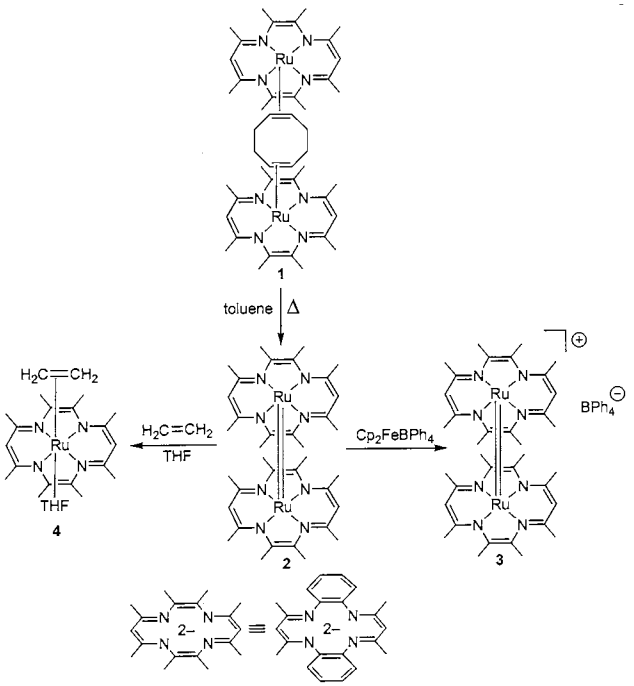

Scheme 1.

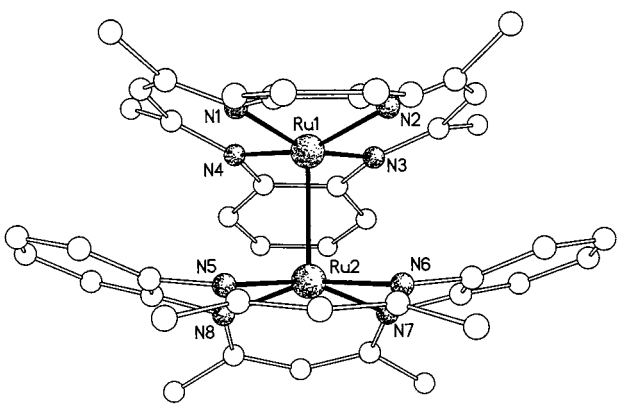

Fig. 1. A drawing of complex **2**. Hydrogens and solvents have been omitted for clarity, while labeling has been used only for nitrogens and metals.

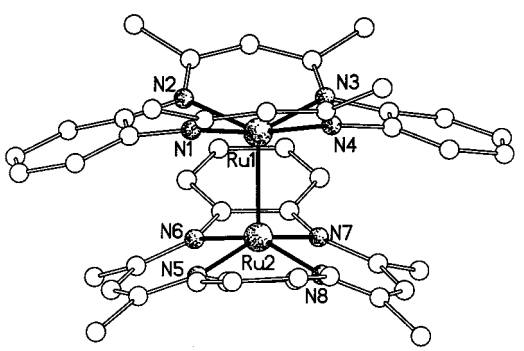

Fig. 2. A drawing of the cation in complex **3**. Hydrogens and solvents have been omitted for clarity, while labeling has been used only for nitrogens and metals.

ment of the cyclooctadiene from the Ru–olefin complex **1** [7] in toluene (see Scheme 1). The dinuclear complex **2** was recrystallized from toluene. The ^{1}H-NMR spectrum carried out in pyridine is in fact not related to the dinuclear complex **2**, but rather to the pyridine derivative [Ru(tmtaa)Py_2] [7], since the metal–metal bond is split by a number of nucleophiles such as CO, pyridine, phosphine [8] and diazoalkanes. In the latter cases, the reaction led to the known [Ru(tmtaa)CR_2] derivatives [7]. Complex **2** has been oxidized in THF to the corresponding monocationic species using Cp_2FeBPh_4. Complex **3** has been obtained as black crystals from a crystallization in toluene. The structural and magnetic relationship between the two dinuclear complexes deserves a detailed discussion. Although the Ru=Ru bond is quite rapidly cleaved in the presence of a number of nucleophiles mentioned above, the reaction of **2** with ethylene carried out in THF was particularly slow. Complex **4** was obtained as brown crystals from THF, the solvent remaining bonded to Ru in the axial position *trans* to ethylene. The diamagnetism is confirmed by the ^{1}H-NMR spectrum, which is in agreement with a pseudo C_{2v} symmetry of the complex and the free rotation of the ethylene around the metal–(C–C) axis.

The structures of **2** and **3** are displayed in Figs. 1 and 2, respectively, while the crystallographic parameters and a selection of bond distances and angles are listed in Tables 1 and 2, respectively. The ORTEP drawings with the numbering scheme and the complete list of structural parameters are reported in Section 4. The overall structures of complexes **2** and **3** are very similar, with each metal in a tetragonal-pyramid environment resembling the analogous Ru–porphyrin derivatives [9]. However, the distortion of the coordination polyhedron is much more pronounced in the tmtaa complexes, with significant out-of-N_4 plane for Ru1 ($-0.349(1)$, **2**; 0.432(1) Å, **3**) and Ru2 (0.338(1), **2**; $-0.425(1)$ Å, **3**). The two tmtaa ligands are rotated with respect to each other by about 90° (N1–Ru1–Ru2–N8 = 90.1(1)°, **2**; N1–Ru1–Ru2–N6 = 92.08(8)°, **3**) and they both show a double saddle-shape conformation, the angles between the two –N=C(Me)–C(H)=C(Me)–N– moieties being 48.9(1), **2**; 46.94(8)°, **3**, and 47.0(1), **2**; 44.98(8)°, **3** and between the N–C_6H_4–N fragments 28.83(8), **2**; 29.23(4), **3** and 30.64(9), **2**; 29.62(4)°, **3** for the two ligands. The Ru–N bond lengths vary, in both complexes, in a very narrow range (2.002(3), **2**; 2.023(2) Å, **3**), and they are comparable with other Ru(tmtaa) complexes [7]. The significance of the Ru–Ru bond distances (Ru1–Ru2, 2.3829(4), **2** and Ru1–Ru2, 2.2782(4) Å, **3**) is discussed below.

The structure of **4** is given in Fig. 3. Ruthenium is in a slightly distorted octahedral geometry, with a small displacement of the metal from the average N_4 plane ($-0.211(1)$ Å). The Ru–N bond distances vary in a

Table 1
Crystal data and details of the structure determination for **2**, **3** and **4**

	2	**3**	**4**
Chemical formula	$C_{44}H_{44}N_8Ru_2 \cdot C_4H_8O \cdot 0.5C_7H_8$	$C_{44}H_{44}N_8Ru_2 \cdot C_{24}H_{20}B \cdot 2C_7H_8$	$C_{28}H_{34}N_4ORu$
Formula weight	1005.18	1390.49	543.66
Crystal system	Monoclinic	Monoclinic	Orthorhombic
Space group	$P2_1/c$	$P2_1/n$	$Pbca$
a (Å)	12.553(2)	14.980(2)	8.8150(10)
b (Å)	32.940(3)	29.184(7)	16.676(4)
c (Å)	11.691(2)	15.009(2)	33.628(6)
α (°)	90	90	90
β (°)	115.52(2)	91.299(10)	90
γ (°)	90	90	90
V (Å^3)	4362.5(11)	6560(2)	4943.3(16)
Z	4	4	8
D_{calc} (g cm^{-3})	1.530	1.408	1.461
μ (mm^{-1})	0.742	0.514	0.663
$F(000)$	2068	2884	2256
Wavelength (Å)	0.71070	0.71070	0.71070
Temperature (K)	190	143	190
θ Range (°)	1.24–25.03	1.53–25.03	1.21–25.02
Measured reflections	22 345	34 342	18 384
Unique reflections	7207 ($R_{int} = 0.0330$)	10 085 ($R_{int} = 0.0332$)	4250 ($R_{int} = 0.0407$)
Unique reflections [$I > 2\sigma(I)$]	6795	8439	3726
Data/parameters	7207/578	10 085/827	4250/308
R [a] [$I > 2\sigma(I)$]	$R = 0.0434$, $wR = 0.1128$	$R = 0.0338$, $wR = 0.0885$	$R = 0.0390$, $wR = 0.1100$
R indices (all data)	$R = 0.0467$, $wR = 0.1335$	$R = 0.0423$, $wR = 0.0947$	$R = 0.0439$, $wR = 0.1310$
Goodness-of-fit	1.138	1.051	1.101
Extinction coefficient	0.0360(11)	0.00258(15)	0.0215(10)
Highest peak and deepest hole (e Å^{-3})	0.857, −0.573	0.556, −0.710	1.227, −0.809

[a] $R = \Sigma||F_o| - |F_c||/\Sigma|F_o|$; $wR = \{\Sigma[w(F_o^2 - F_c^2)^2]/\Sigma[w(F_o^2)^2]\}^{1/2}$.

Table 2
Selected bond distances (Å) for complexes **2**, **3**, and **4**

2					
Ru1–N1	2.019(3)	Ru1–N4	2.011(3)	Ru2–N6	2.013(3)
Ru1–N2	2.002(3)	Ru1–Ru2	2.3829(4)	Ru2–N7	2.010(3)
Ru1–N3	2.019(3)	Ru2–N5	2.014(3)	Ru2–N8	2.005(3)
3					
Ru1–N1	2.023(2)	Ru1–N4	2.003(2)	Ru2–N6	2.011(2)
Ru1–N2	2.006(2)	Ru1–Ru2	2.2782(4)	Ru2–N7	2.019(2)
Ru1–N3	2.018(2)	Ru2–N5	2.022(2)	Ru2–N8	2.005(2)
4					
Ru1–N1	2.022(2)	Ru1–N4	2.025(2)	Ru1–O1	2.247(2)
Ru1–N2	2.037(2)	Ru1–C23	2.120(3)	C23–C24	1.384(5)
Ru1–N3	2.025(2)	Ru1–C24	2.130(3)		

very limited range (2.022(2)–2.037(2) Å) and the ligand adopts the usual double saddle-shape conformation, the angle between the two –N=C(Me)–C(H)=C(Me)–N– moieties being (39.3(1)°), and between the two N–C_6H_4–N fragments 35.24(8)°. As expected, the angle between the least-square planes containing the N_4 core and the ethylene (ruthenium included) is ~90° (89.7(1)°). The axial positions of the octahedron are occupied by the centroid of an ethylene molecule and by an oxygen of a THF molecule (Ru1–η^2(C23, C24), 2.009(2); Ru1–O1, 2.247(2) Å). Some lengthening of the C=C bond of ethylene (1.384(5) Å) upon coordination to ruthenium has been observed.

Both complexes **2** and **3** are paramagnetic. The temperature dependence of the magnetic moments of **2** is illustrated in Fig. 4. We see that the magnetic moment per ruthenium is almost constant between 50 and 300 K, with a room-temperature value of 1.96 μ_B at 298 K, suddenly decreasing below 50 K, reaching 0.23 at 2 K. The room-temperature value of the effective magnetic moment is consistent with an $S = 1$ ground state for the dinuclear unit and the decrease at low temperature can

be attributed to a large zero-field splitting. The magnetic data have been fit with the axial spin Hamiltonian [10] $H = \mu_B g \mathbf{H} \cdot S + D[S_z^2 - S(S+1)/3]$, where $S = 1$, g is the average g-factor, and D is the zero-field splitting constant. This spin-Hamiltonian leads for the magnetic susceptibility to the following equation:

$$\chi_{dim} = \frac{2Ng^2\mu_B^2}{3kT} \frac{\exp(-x) + (2/x)[1 - \exp(-x)]}{1 + 2\exp(-x)}$$

where $x = D/kT$ [10]. A good fit has been obtained accounting for the presence of a small amount of paramagnetic impurities. In this case, the most probable impurity is the oxidation product **3**, for which we assume $S_{imp} = 1/2$ and $g_{imp} = 2.0$, so that the final expression for the magnetic susceptibility can be written $\chi = (1-p)\chi_{dim} + p\chi_{imp}$, where p is the mole fraction of the impurity and

$$\chi_{imp} = \frac{Ng_{imp}^2\mu_B^2 S_{imp}(S_{imp}+1)}{3kT}$$

The best fit to this expression of the experimental data leads to the following parameters: $g = 2.01$, $D = 196\ cm^{-1}$ and $p = 0.6\%$ (see solid line in Fig. 4).

The value obtained for the zero-field splitting constant, 196 cm^{-1}, is close to those observed for analogous $[Ru(porphyrin)]_2$ dinuclear complexes, i.e. 240 cm^{-1} for $[Ru(OEP)]_2$ and 280 cm^{-1} for $[Ru(OETAP)]_2$ [11], or for ruthenium carboxylate dinuclear complexes, $[Ru(O_2CR)_2]_2$ [12].

The magnetic moment of **3** is almost constant in the temperature range 4–300 K with a value of ca. 1.50 μ_B, which, although lower than the spin-only value, clearly indicates a doublet ground state. Earlier measurements by Warren and Goedken [6] had given a room-temperature value of 1.55 μ_B in agreement with our data, although no variable temperature investigation had been performed.

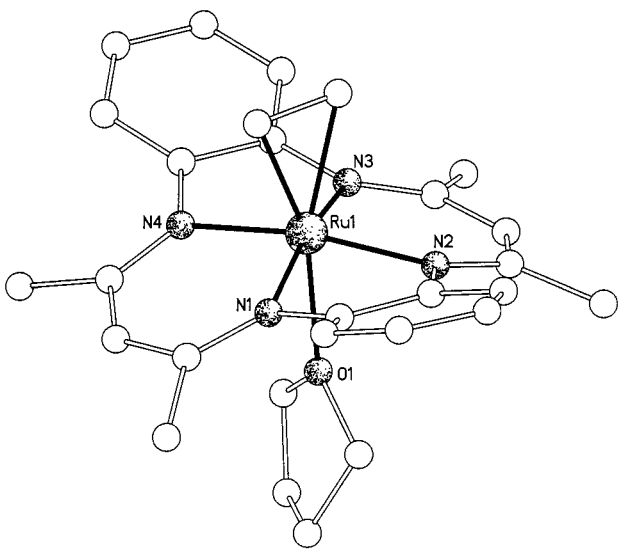

Fig. 3. A drawing of complex **4**. Hydrogens have been omitted for clarity.

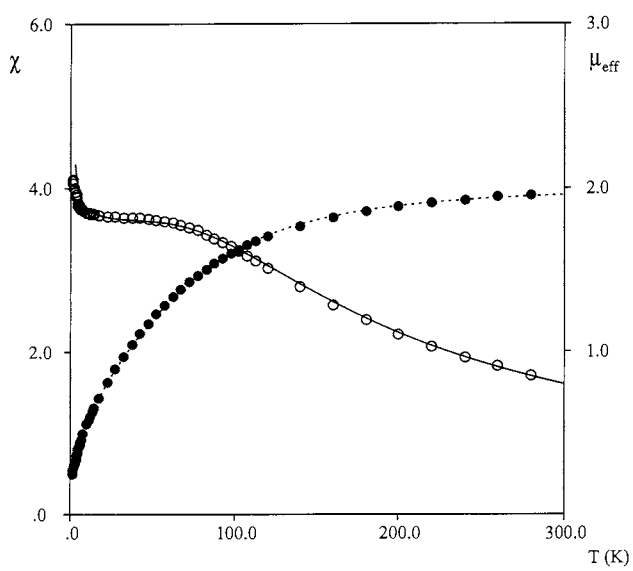

Fig. 4. Temperature dependence of the magnetic susceptibility (○) and effective magnetic moment (●) per ruthenium in complex **2**.

2.2. Electronic structure

Extended Hückel calculations [13] have been performed to elucidate the nature of the metal–ethylene bonding in **4** and to give a better understanding of the metal–metal bonding as well as the magnetic behavior of the ruthenium dinuclear complexes **2** and **3**.

The electronic structure of the η^2-ethylene complex **4** is analyzed in terms of the interactions between the frontier orbitals of the $[Ru(tmtaa)(H_2O)]$ metal fragment and the ethylene moiety. The molecular orbitals of the $[Ru(tmtaa)(H_2O)]$ fragment are constructed using a two-step approach. We first considered the [Ru(tmtaa)] fragment and then the effect on its molecular orbitals of the coordination of an axial THF ligand, which has been simulated with a water molecule. The molecular orbitals of the [Ru(tmtaa)] fragment have already been discussed [7b], and are reported here on the left of Fig. 5. Due to the strong mixing between ruthenium and tmtaa ligand orbitals, no pure d-orbitals can be assigned to the frontier orbitals of this fragment. However, five MOs with significant metal d-character can be identified. These are the three highest occupied orbitals $a_1(d_{z^2})$, $b_2(d_{yz})$, $b_1(d_{xz})$, and the lowest unoccupied orbital $a_1(d_{x^2-y^2})$ lying in the N_4 ligand plane. The fifth orbital is the $a_2(d_{xy})$, which points more directly towards the nitrogen atoms of tmtaa, and hence is pushed to a still higher energy. In the second column of Fig. 5 we illustrate the effect of the coordination of a water molecule, which leads to the energy rise of the $a_1(d_{z^2})$, becoming the LUMO in the $[Ru(tmtaa)(H_2O)]$ fragment. On the extreme right of Fig. 5 the frontier

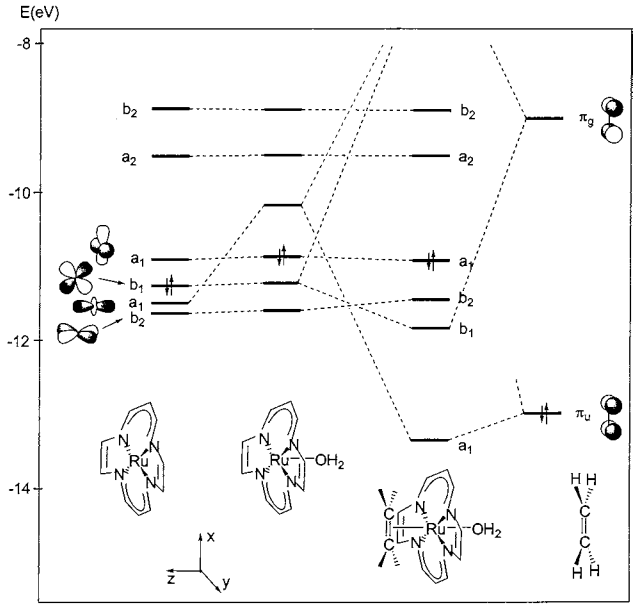

Fig. 5. Orbital interaction diagram for the valence orbitals of complex **4**.

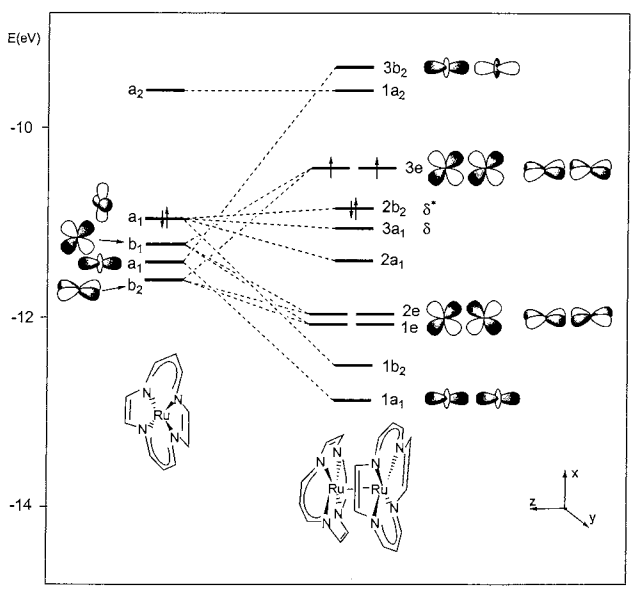

Fig. 6. Orbital interaction diagram for the valence orbitals of complex **2**.

orbitals of C_2H_4, i.e. the occupied π_u and the empty π_g, are shown. The interaction between the [Ru(tmtaa)(H_2O)] fragment and the ethylene unit is illustrated by the molecular orbital diagram in the third column of Fig. 5. Fig. 5 indicates that there is a strong interaction between the empty σ-acceptor $1a_1(d_{z^2})$ metal orbital and the π_u orbital of C_2H_4, and between the filled $1b_1(d_{xz})$ and the π-acceptor π_g.

The experimental X-ray structure of **4** indicates that the ethylene molecule is oriented with its axis in the *xz* symmetry plane bisecting the diiminato rings. However, in principle the π* orbital of C_2H_4 could interact with both the doubly occupied $b_1(d_{xz})$, $b_2(d_{yz})$ metal orbitals leading to different orientations of the ethylene moiety with the main axis lying in the *xz* or *yz* planes, respectively. In agreement with the experimental X-ray results, the former orientation has been calculated to be ca 0.5 eV more stable, probably due to the more favorable energy match of the ethylene π* orbital with the higher-lying $1b_1(d_{xz})$. Our calculations also give an estimate of the energy barrier for the rotation of ethylene around the bond axis of about 11 kcal mol^{-1}, thus suggesting an essentially free rotation of the organic fragment at room temperature, in good agreement with the ^{1}H-NMR at 298 K.

The interaction diagram of the two [Ru(tmtaa)] fragments in the neutral dinuclear complex **2** is illustrated in Fig. 6. Due to the large mixing of the π system of the tmtaa ligand with the d-metal orbitals, the metal–metal bonding character is distributed over several orbitals. The low lying $1a_1$ orbital describes the Ru–Ru σ-bond, while its antibonding σ* counterpart is described by the empty $3b_2$. The Ru–Ru π bonding is distributed over the two 1e and 2e orbitals, while the 3e has a mainly π* character. The Ru–Ru δ-type interaction is distributed over the $1b_2$–$2b_2$ (δ*) and $2a_1$–$3a_1$ (δ) orbitals and is expected to give a minor contribution to metal–metal bonding. Our calculation indicates a mainly Ru–Ru $\sigma^2\pi^4\delta^2\delta^{*2}\pi^{*2}$ electron configuration and suggests, therefore, a ruthenium–ruthenium double-bond character which is consistent with the observed metal–metal distance of 2.3829(4) Å. Indeed, this value is only slightly longer than those observed for other doubly bonded Ru_2^{4+} complexes [14] (falling in the range 2.25–2.35), but the slight lengthening can be attributed to the steric repulsion between the macrocyclic ligands. In the ideal D_{2d} geometry the doubly degenerate 3e orbital is occupied by two electrons indicating a triplet ground state, in agreement with the observed magnetic behavior.

The same molecular orbital scheme of Fig. 6, after removal of one electron, applies to the $[Ru(tmtaa)]_2^+$ cation, which therefore has a $\sigma^2\pi^4\delta^2\delta^{*2}\pi^{*1}$ electron configuration. The removal of an electron from the π* orbital is consistent with the decrease of 0.105 Å observed for the Ru–Ru bond length [3,14]. The molecular orbital scheme in Fig. 6 indicates a quite clear separation (ca. 0.5 eV) between the π* and δ* orbitals, thus suggesting a doublet ground state in agreement with the magnetic evidence. This is the same ground state observed for the Ru_2^{5+} core in analogous $[Ru(porphyrin)]_2^+$ complexes [2b,3]. On the other hand, a different behavior is observed for carboxylate and amido bridged Ru_2^{5+} cores which, due to a quasi degeneracy of π* and δ*, show a quartet ground state [15].

3. Experimental

3.1. General procedures

All operations were carried out under an atmosphere of purified nitrogen. All solvents were purified by standard methods and freshly distilled prior to use. Infrared spectra were recorded with a Perkin–Elmer FT 1600 spectrophotometer, NMR spectra were recorded on AC-200 and DPX-400 Bruker spectrometers. Magnetic susceptibility measurements were collected in the temperature range 2–300 K on a MPMS5 SQUID susceptometer (Quantum Design Inc.), operating at a magnetic field strength of 1 kOe. Corrections were applied for diamagnetism calculated from the Pascal constants. Finally, the synthesis of **1** was carried out according to Ref. [7b].

3.2. Synthesis of *2*

A red suspension of $[Ru(tmtaa)(COD)_{0.5}(THF)_{0.5}]$ (3.64 g, 6.6 mmol) in toluene (100 ml) was refluxed for 2 h, after which the black crystalline product obtained was collected and dried in vacuo (2.40 g, 74%). Crystals suitable for X-ray analysis were grown in a toluene solution. (Found: C, 62.07; H, 5.26; N, 11.56. Anal. Calc. for $C_{51}H_{52}N_8Ru_2$: C, 62.56; H, 5.35; N, 11.44%). ^{1}H-NMR (pyridine-d_5, 200 MHz, 298 K, ppm): δ 1.95 (s, 24H, CH_3); 2.20 (s, 3H, toluene); 4.04 (s, 4H, CH); 6.32 (m, 8H, Ar); 6.75 (m, 8H, Ar); 7.17 (m, 5H, toluene). IR (Nujol, ν_{max} cm^{-1}): 1572 (w), 1504 (m), 1371 (s), 1287 (m), 1259 (w), 1190 (m), 1031 (m), 798 (w), 774 (w), 738 (s), 544 (w), 503 (w). UV (THF) λ_{max} 212 nm (ε 55 000 cm^{-1} M^{-1}); 224 sh (45 580); 258 (32 520); 298 (46 800); 324 sh (33 300); 404 sh (17 540); 424 (23 160); 466 sh (8770); 556 (6500); 604 sh (5030).

3.3. Synthesis of *3*

Cp_2FeBPh_4 (1.8 g, 3.5 mmol) was added to a black suspension of $[Ru(tmtaa)]_2$·tol (3.5 g, 3.5 mmol) in THF (100 ml). The suspension was stirred overnight and the black product obtained was collected and dried in vacuo (3.6 g, 78%). Crystals suitable for X-ray analysis were grown in a toluene solution. (Found: C, 67.62; H, 5.95; N, 8.56. Anal. Calc. for $C_{72}H_{72}N_8BORu_2$: C, 67.65; H, 5.68; N, 8.76%). IR (Nujol, ν_{max} cm^{-1}): 1942 (w), 1876 (w), 1820 (w), 1576 (m), 1511 (s), 1425 (s), 1350 (s), 1280 (m), 1195 (m), 1124 (w), 1058 (m), 1030 (m).

3.4. Synthesis of *4*

A black suspension of $[Ru(tmtaa)]_2$·tol (2.81 g, 2.87 mmol) in THF (150 ml) was stirred under ethylene for 3 weeks. The resulting red solution was filtered and the solvent was evaporated. Then *n*-hexane (50 ml) was added and a brown product obtained, which was collected and dried in vacuo (1.94 g, 72%). Crystals suitable for X-ray analysis were grown in a THF solution. (Found: C, 60.68; H, 5.83; N, 11.04. Anal. Calc. for $C_{28}H_{34}N_4ORu$: C, 61.86; H, 6.30; N, 10.30%). ^{1}H-NMR (C_6D_6, 400 MHz, 298 K, ppm): δ 2.24 (s, 12H, CH_3); 2.58 (s, 4H, CH_2); 5.11 (s, 2H, CH); 6.52–6.55 (m, 4H, Ar); 6.82–6.87 (m, 4H, Ar). ^{13}C-NMR (C_6D_6, 100.6 MHz, 298 K, ppm): δ 25.56 (CH_3); 54.56 (br, CH_2); 111.27 (CH); 121.16 (CH Ar); 121.63 (CH Ar); 149.10 (C_{quat}); 154.51 (C_{quat}).

3.5. X-ray experimental

Suitable crystals of **2**, **3**, and **4** were mounted in glass capillaries and sealed under nitrogen. Data concerning crystals, data collection and structure refinement are listed in Table 1. Data collections were performed at 190 K (**2** and **4**) and at 143 K (**3**) on a mar345 Imaging Plate Detector. Data reduction was carried out with marHKL, Release 1.9.1 [16]. No absorption correction was applied. Structure solutions for all compounds were determined with ab initio direct methods [17]. All structures were refined using the full-matrix least-squares on F^2 with all non-H atoms anisotropically defined. H atoms were placed in calculated positions using the riding model with $U_{iso} = a^* U_{eq}(C)$ (where a is 1.5 for methyl hydrogens and 1.2 for others, while C is the parent carbon atom), and in some cases for hydrogens belonging to solvent molecules a common isotropic displacement parameter ($U_{iso} = 0.08$ Å^2) was used. Structure solutions, refinements, molecular graphics and geometrical calculations have been carried out on all structures with the SHELXTL software package [18]. Final atomic coordinates, thermal and geometrical parameters and hydrogen coordinates are listed in Section 4.

4. Supplementary information

ORTEP drawings with the numbering scheme, tables giving crystal data and structure refinement, atomic coordinates, bond length and angles, anisotropic displacement parameters, hydrogen coordinates and isotropic displacement parameters, and torsion angles for **2**, **3**, and **4** (25 pages). Crystallographic data (excluding structure factors) for the structures reported in this paper have been deposited with the Cambridge Crystallographic Data Centre as supplementary publication nos. CCDC-127331 for **2**, CCDC-127332 for **3** and CCDC-127333 for **4**. Copies of the data can be obtained free of charge on application to CCDC, 12 Union Road, Cambridge CB2 1EZ, UK (fax: +44-1223-336033; e-mail: deposit@ccdc.cam.ac.uk; http://www.ccdc.cam.ac.uk).

Acknowledgements

We thank the 'Fonds National Suisse de la Recherche Scientifique' (Bern, Switzerland, Grant no. 20-53336.98), Ciba Specialty Chemicals S.A. (Basel, Switzerland), Action COST D9 (European Program for Scientific Research, OFES no. C98.008) and Fondation Herbette (Université de Lausanne, N.R.) for financial support.

References

[1] J.P. Collman, H. Arnold, Acc. Chem. Res. 16 (1993) 586.
[2] (a) H. Asahina, M.B. Zisk, B. Hedman, J.T. McDevitt, J.P. Collman, K.O. Hodgson, J. Chem. Soc. Chem. Commun. (1989) 1360. (b) C.D. Tait, J.M. Garner, J.P. Collman, A.P. Sattelberger, W.H. Woodruff, J. Am. Chem. Soc. 111 (1989) 7806. (c) J.P. Collman, J.W. Prodolliet, C.R. Leidner, J. Am. Chem. Soc. 108 (1986) 2916. (d) J.P. Collman, C.E. Barnes, T.J. Collins, P.J. Brothers, J. Am. Chem. Soc. 103 (1981) 7030.
[3] J.P. Collman, S.T. Harford, Inorg. Chem. 37 (1998) 4152.
[4] Some leading references in the use of $[tmtaa]^{2-}$ as ancillary ligand in the organometallic chemistry of the early transition metals are: (a) V.L. Goedken, J.A. Ladd, J. Chem. Soc. Chem. Commun. (1981) 910; J. Chem. Soc. Chem. Commun. (1982) 142. (b) C. Floriani, S. Ciurli, A. Chiesi-Villa, C. Guastini, Angew. Chem. Int. Ed. Engl. 26 (1987) 70. (c) E. Solari, S. De Angelis, C. Floriani, A. Chiesi-Villa, C. Rizzoli, Inorg. Chem. 31 (1992) 96. (d) S. De Angelis, E. Solari, E. Gallo, C. Floriani, A. Chiesi-Villa, C. Rizzoli, Inorg. Chem. 31 (1992) 2520. (e) L. Giannini, E. Solari, C. Floriani, A. Chiesi-Villa, C. Rizzoli, Angew. Chem. Int. Ed. Engl. 33 (1994) 2204. (f) L. Giannini, E. Solari, S. De Angelis, T. Ward, C. Floriani, A. Chiesi-Villa, C. Rizzoli, J. Am. Chem. Soc. 117 (1995) 5801. (g) D.G. Black, D.C. Swenson, R.F. Jordan, Organometallics 14 (1995) 3539. (h) A.J. Blake, P. Mountford, G.I. Nikonov, D. Swallow, Chem. Commun. (Cambridge) (1996) 1835. (i) H. Schumann, Inorg. Chem. 35 (1996) 1808. (j) G.I. Nikonov, A.J. Blake, P. Mountford, Inorg. Chem. 36 (1997) 1107. (k) D.G. Black, R.F. Jordan, R.D. Rogers, Inorg. Chem. 36 (1997) 103. (l) A. Martin, R. Uhrhammer, T.G. Gardner, R.F. Jordan, Organometallics 17 (1998) 382. (m) P. Mountford, Chem. Soc. Rev. 27 (1998) 105.
[5] (a) F.A. Cotton, J. Czuchajowska, Polyhedron 9 (1990) 2553. (b) F.A. Cotton, J. Czuchajowska, J. Am. Chem. Soc. 113 (1991) 3427.
[6] L.F. Warren, V.L. Goedken, J. Chem. Soc. Chem. Commun. (1978) 909.
[7] (a) A. Klose, E. Solari, C. Floriani, S. Geremia, L. Randaccio, Angew. Chem. Int. Ed. Engl. 37 (1998) 148. (b) A. Klose, J. Hesschenbrouck, C. Floriani, N. Re, S. Geremia, L. Randaccio, Organometallics 18 (1999) 360.
[8] For the synthesis end the structure of $[Ru(tmtaa)(PR_3)_2]$, see: (a) F.A. Cotton, J. Czuchajowska, Polyhedron 9 (1990) 1221. (b) L. Luo, E.D. Stevens, S.P. Nolan, Inorg. Chem. 35 (1996) 252.
[9] J.P. Collman, C.E. Barnes, P.N. Swepston, J.A. Ibers, J. Am. Chem. Soc. 106 (1984) 3500.
[10] O. Kahn, Molecular Magnetism, VCH, New York, 1992.
[11] H.A. Godwin, J.P. Collman, J.-C. Marchon, P. Maldivi, G.T. Yee, B.J. Conklin, Inorg. Chem. 36 (1997) 399.
[12] F.A. Cotton, V.M. Miskowski, B. Zhong, J. Am. Chem. Soc. 111 (1989) 6177.
[13] (a) R. Hoffmann, W.N. Lipscomb, J. Chem. Phys. 36 (1962) 2179. (b) R. Hoffmann, J. Chem. Phys. 39 (1963) 1397.
[14] F.A. Cotton, Multiple Bonds between Metal Atoms, Clarendon Press, Oxford, 1983.
[15] (a) M.A.S. Aquino, Coord. Chem. Rev. 170 (1998) 141. (b) A. Carvill, P. Higgins, G.M. McCann, H. Ryan, A. Shiels, J. Chem. Soc. Dalton Trans. (1989) 2435. (c) B.K. Das, A.R. Chakravarty, Polyhedron 7 (1988) 685. (d) A.R. Chakravarty, F.A. Cotton, Inorg. Chim. Acta 113 (1986) 19. (e) A.R. Chakravarty, F.A. Cotton, D.A. Tocher, Inorg. Chem. 24 (1985) 172.
[16] Z. Otwinowski, W. Minor, Methods in enzymology, in: C.W. Carter, R.M. Sweet (Eds.), Macromolecular Crystallography, vol. 276, Academic Press, New York, 1997, p. 307, part A.
[17] G.M. Sheldrick, Acta Crystallogr. Sect. A 46 (1990) 467.
[18] SHELXTL Software Package, Release 5.1., Bruker AXS Inc., Madison, WI, 1997.